

000 001 Q-FSRU: QUANTUM-AUGMENTED FREQUENCY- 002 SPECTRAL FUSION FOR MEDICAL VISUAL QUESTION 003 ANSWERING 004 005

006 **Anonymous authors**
007 Paper under double-blind review
008
009
010
011
012

ABSTRACT

013 Solving tough clinical questions that require both image and text understanding
014 is still a major challenge in healthcare AI. In this work, we propose Q-FSRU, a
015 new model that combines Frequency Spectrum Representation and Fusion (FSRU)
016 with a method called Quantum Retrieval-Augmented Generation (Quantum RAG)
017 for medical Visual Question Answering (VQA). The model takes in features from
018 medical images and related text, then shifts them into the frequency domain using
019 Fast Fourier Transform (FFT). This helps it focus on more meaningful data and
020 filter out noise or less useful information. To improve accuracy and ensure that
021 answers are based on real knowledge, we add a quantum inspired retrieval system.
022 It fetches useful medical facts from external sources using quantum-based
023 similarity techniques. These details are then merged with the frequency-based
024 features for stronger reasoning. We evaluated our model using the VQA-RAD
025 dataset, which includes real radiology images and questions. The results showed
026 that Q-FSRU outperforms earlier models, especially on complex cases needing
027 image text reasoning. The mix of frequency and quantum information improves
028 both performance and explainability. Overall, this approach offers a promising
029 way to build smart, clear, and helpful AI tools for doctors.
030
031

1 INTRODUCTION

032 Medical visual question answering (Med-VQA) represents an emerging interdisciplinary challenge
033 that sits at the intersection of computer vision, natural language processing, and clinical decision-
034 making (Lin et al., 2023). In real-world clinical environments, radiologists and medical practitioners
035 frequently interact with imaging studies by formulating diagnostic questions such as 'Is there ev-
036 idence of a pulmonary nodule?' or 'Does this MRI show signs of cerebral edema?'. Addressing
037 such queries demands not only sophisticated understanding of visual content in medical images
038 but also deep contextual knowledge and nuanced language comprehension (Lau et al., 2018). The
039 development of AI systems for Med-VQA faces several unique challenges that distinguish it from
040 general-domain VQA. These include severe data scarcity due to privacy concerns, highly specialized
041 medical terminology, complex imaging modalities (CT, MRI, X-ray, etc.), and the critical nature of
042 medical decision-making where errors can have serious consequences. While transformer-based
043 architectures and cross-modal fusion techniques have shown remarkable progress in general VQA
044 benchmarks (Antol et al., 2015; Vaswani et al., 2017), their direct application to medical domains
045 has yielded limited success. Recent medical-specific vision-language models such as LLaVA-Med
046 (Li et al., 2023), STLLaVA-Med (Sun et al., 2024a), and concept-aligned approaches like MMCAP
047 (Yan et al., 2024) have improved domain adaptation, but they predominantly operate in the spatial
048 domain, potentially overlooking subtle frequency-based patterns that are particularly relevant in
049 medical imaging. Most current Med-VQA models rely on convolutional or attention-based feature
050 extractors that process images in the spatial domain. While effective for capturing local structures,
051 these approaches may miss global contextual cues embedded in frequency spectra that are especially
052 important for detecting pathological patterns in medical images (Cai et al., 2023). Concurrently,
053 retrieval-augmented methods that incorporate external knowledge have shown promise in improving
factual grounding (Lewis et al., 2021), but they typically rely on classical similarity measures
like cosine similarity, which may not fully capture the complex semantic relationships required for

054 clinical reasoning. Recent work has demonstrated the effectiveness of frequency-domain repres-
 055 sentations in various multimodal tasks. As shown by Lao et al. (2024), frequency spectrum analysis
 056 can be more effective for multimodal representation and fusion in rumor detection, while Cai et al.
 057 (2023) proposed FDTrans, a frequency-domain transformer for multimodal medical image analysis.
 058 In medical imaging specifically, frequency-aware components have been incorporated into architec-
 059 tures like FreqU-FNet (Xing, 2025) for segmentation tasks. However, these approaches have not
 060 been comprehensively explored for medical VQA, where the combination of visual and textual fre-
 061 quency analysis could potentially capture complementary diagnostic information. To address these
 062 limitations, we propose Q-FSRU, a novel framework that combines Frequency Spectrum Repre-
 063 sentation and Fusion (FSRU) with a Quantum-inspired Retrieval-Augmented Generation (Quantum
 064 RAG) mechanism for medical VQA. Our approach is motivated by two key insights: first, that
 065 transforming multimodal features into the frequency domain can help capture global contextual pat-
 066 terns often missed by spatial processing; and second, that quantum-inspired similarity measures
 067 may offer advantages over classical retrieval methods for capturing nuanced semantic relationships
 068 in medical knowledge. The frequency fusion component of Q-FSRU transforms input features from
 069 both image and text modalities using Fast Fourier Transform (FFT), allowing the model to selec-
 070 tively attend to salient frequency-domain signals while suppressing irrelevant spatial noise. This
 071 spectral transformation enables our model to capture global contextual cues that are particularly
 072 valuable for identifying pathological patterns in medical images. To complement this, we integrate
 073 a quantum-inspired retrieval mechanism that fetches relevant external clinical knowledge based on
 074 amplitude-based similarity principles, helping ground the model’s reasoning in verifiable medical
 075 facts. Our contributions can be summarized as follows:
 076

- 077 1. We introduce a novel frequency domain fusion framework for medical VQA that transforms
 078 visual and textual features using FFT to capture complementary spectral patterns.
- 079 2. We propose a quantum-inspired retrieval mechanism that enhances factual grounding by
 080 retrieving relevant medical knowledge based on amplitude similarity measures.
- 081 3. We demonstrate through extensive experiments on the VQA-RAD dataset that our approach
 082 achieves competitive performance compared to existing methods, with particular strengths
 083 in complex reasoning cases.
- 084 4. We provide analysis showing that the combination of spectral processing and knowledge
 085 retrieval improves both performance and interpretability, making the model more suitable
 086 for clinical applications.

087 2 RELATED WORK

088 2.1 MEDICAL VISUAL QUESTION ANSWERING

089 Medical Visual Question Answering (Med-VQA) is a core challenge in healthcare AI, requiring joint
 090 reasoning over medical images and domain-specific language. Early efforts adapted general VQA
 091 frameworks to clinical data but struggled with specialized terminology and imaging complexity (Lau
 092 et al., 2018; Lin et al., 2023). More recent approaches such as STLLaVA-Med (Sun et al., 2024b)
 093 leverage large language models and self-training strategies, achieving notable gains through domain
 094 adaptation. However, most existing methods operate solely in the spatial domain and have limited
 095 ability to capture frequency-based patterns that may hold diagnostic value. Furthermore, knowledge
 096 integration remains constrained by conventional retrieval techniques. To address these gaps, we pro-
 097 pose a framework that combines frequency-domain representations with quantum-inspired retrieval
 098 to better align image-text reasoning with clinical requirements.

099 2.2 FREQUENCY-DOMAIN REPRESENTATIONS

100 Frequency-domain analysis has demonstrated value across various computer vision applications.
 101 In medical imaging specifically, Cai et al. (2023) developed FDTrans, a frequency-domain trans-
 102 former that captures complementary information to spatial representations for diagnostic tasks. This
 103 work highlights how spectral features can enhance medical image analysis beyond conventional
 104 approaches. Xing (2025) incorporated frequency-aware components into segmentation architec-
 105 tures, showing improved performance on imbalanced medical datasets through better global pattern

108 capture. The work by Lao et al. (2024) is particularly relevant, showing that frequency spectrum
 109 analysis improves multimodal representation and fusion for rumor detection. However, their focus
 110 on social media content differs from our medical application, and they did not explore knowledge re-
 111 trieval mechanisms. Our approach extends this foundation by applying frequency-domain methods
 112 specifically to medical visual question answering while incorporating novel retrieval components.
 113

114 2.3 QUANTUM-INSPIRED METHODS IN INFORMATION RETRIEVAL

115 Quantum-inspired approaches to information retrieval have developed over the past two decades,
 116 offering alternative mathematical frameworks for similarity measurement and representation learn-
 117 ing. As surveyed by Upadhyay et al. (2021), quantum theory provides a generalized probability and
 118 logic framework that has shown promise for developing more dynamic and context-aware retrieval
 119 systems. This established research area offers theoretical foundations for our quantum-inspired
 120 retrieval approach. Recent applications demonstrate the practical value of quantum-inspired meth-
 121 ods. Kaneko et al. (2025) proposed quantum-inspired projection heads and similarity metrics for
 122 representation learning, showing competitive performance with significantly reduced parameters
 123 compared to classical methods. Their work on embedding compression for information retrieval
 124 tasks provides direct precedent for our quantum-inspired similarity approach. In computer vision
 125 applications, Nguyen et al. (2025) developed Quantum-Brain, a quantum-inspired neural network
 126 for vision-brain understanding problems. Their approach demonstrates how quantum principles
 127 can enhance connectivity learning in neural representations, particularly relevant for tasks requiring
 128 complex relationship modeling. This work shows the applicability of quantum-inspired methods
 129 to vision-related tasks similar to medical visual question answering. These quantum-inspired ap-
 130 proaches differ from our work in their specific applications, but collectively establish the viability of
 131 quantum principles for enhancing similarity measurement and representation learning. Our con-
 132 tribution lies in adapting these principles specifically for medical knowledge retrieval in visual question
 133 answering contexts.
 134

135 2.4 KNOWLEDGE RETRIEVAL IN VISUAL QUESTION ANSWERING

136 Retrieval-augmented methods have become increasingly important for tasks requiring external
 137 knowledge integration. The foundational work by Lewis et al. (2021) established retrieval-
 138 augmented generation as a powerful approach for knowledge-intensive tasks. In medical contexts,
 139 however, standard retrieval methods often struggle with the nuanced relationships required for clin-
 140 ical reasoning. Recent multimodal research continues to advance integration techniques. Huang
 141 et al. (2025) explored pixel-level insight for biomedical applications, while datasets like MMVP
 142 from Zhang et al. (2024) provide resources for evaluating multimodal systems. These contributions
 143 highlight the ongoing importance of robust multimodal integration in healthcare applications.
 144

145 2.4.1 RESEARCH CONTRIBUTIONS

146 Our work distinguishes itself from existing approaches through several key contributions. While
 147 prior frequency-domain methods that focus on single modalities or non-medical applications, we
 148 specifically address medical visual question answering with integrated frequency processing. Com-
 149 pared to standard retrieval approaches, we introduce quantum-inspired similarity measures grounded
 150 in established research. And unlike conventional medical visual question answering systems, we
 151 combine both frequency-domain analysis and quantum-inspired retrieval within a unified frame-
 152 work, Q-FSRU designed for clinical applications. The integration of these components addresses
 153 limitations in current medical visual question answering systems while building on established re-
 154 search in frequency-domain processing and quantum-inspired information retrieval. This combi-
 155 nation represents a novel approach to enhancing both performance and interpretability in medical
 156 artificial intelligence systems.
 157

158 3 PROBLEM DEFINITION

159
 160 We formulate medical visual question answering as a multimodal classification task. Given the
 161 VQA-RAD dataset $\mathcal{D} = \{(I_i, Q_i, y_i)\}_{i=1}^N$, where $I_i \in \mathbb{R}^{H \times W \times 3}$ represents a medical image, Q_i
 denotes a clinical question, and $y_i \in \{0, 1, \dots, C-1\}$ indicates the answer class among C possible

162 categories. The VQA-RAD dataset contains both binary (“yes”/“no”) and open-ended questions;
 163 we focus on the subset with categorical answers suitable for classification, filtering questions to
 164 those with discrete answer classes. The objective is to learn a mapping function $f : (I_i, Q_i) \rightarrow$
 165 \hat{y}_i that predicts the correct answer. Our Q-FSRU model enhances this mapping through two key
 166 components:

- 168 • **Frequency-spectral fusion:** $z_i^{\text{freq}} = f_{\text{FSRU}}(I_i, Q_i)$ transforms multimodal features into the
 169 frequency domain
- 170 • **Knowledge retrieval:** $k_i \in \mathbb{R}^d$ represents relevant medical knowledge retrieved from ex-
 171 ternal corpora
- 172 • **Feature integration:** $\hat{y}_i = f_{\theta}(z_i^{\text{freq}}, k_i) = \text{MLP}([z_i^{\text{freq}} \| k_i])$ where $\|$ denotes concatenation
 173

174 The model is trained to minimize a combined objective function:

$$175 \mathcal{L} = \mathcal{L}_{\text{CE}}(\hat{y}_i, y_i) + \alpha \mathcal{L}_{\text{intra}} + \beta \mathcal{L}_{\text{cross}}$$

177 where \mathcal{L}_{CE} represents the cross-entropy classification loss, $\mathcal{L}_{\text{intra}}$ and $\mathcal{L}_{\text{cross}}$ denote intra-modal and
 178 cross-modal contrastive losses respectively, and α, β are hyperparameters that balance the con-
 179 trastive objectives. leverages frequency-domain patterns and external medical knowledge while pre-
 180 serving the discriminative power needed for accurate clinical question answering.

182 4 METHODOLOGY

184 4.1 MODEL ARCHITECTURE OVERVIEW

186 The Q-FSRU framework integrates four core components: (1) multimodal feature extraction, (2)
 187 frequency-domain processing via Fast Fourier Transform, (3) quantum-inspired knowledge retrieval,
 188 and (4) multimodal fusion with contrastive learning. The architecture processes medical images
 189 and clinical questions through a sequential pipeline where frequency-domain enhancement precedes
 190 knowledge retrieval, ensuring optimal feature representation before external knowledge integration.

192 4.2 MULTIMODAL FEATURE EXTRACTION

194 4.2.1 TEXT FEATURE ENCODING

195 Clinical questions are processed using a pretrained word embedding approach. Given a tokenized
 196 question $Q = [w_1, w_2, \dots, w_L]$ of length L , each word w_i is mapped to a 300-dimensional vector
 197 using domain-specific embeddings:

$$199 E_{\text{text}} = \text{Embedding}(Q) \in \mathbb{R}^{L \times 300}$$

200 The sequence undergoes mean pooling across the temporal dimension followed by linear projection:

$$202 \vec{t} = W_t \cdot \left(\frac{1}{L} \sum_{i=1}^L \vec{e}_i \right) + b_t \in \mathbb{R}^{d_{\text{model}}}$$

205 where $W_t \in \mathbb{R}^{d_{\text{model}} \times 300}$, $b_t \in \mathbb{R}^{d_{\text{model}}}$, and $d_{\text{model}} = 256$.

207 4.2.2 IMAGE FEATURE ENCODING

208 Medical images are processed using a Vision Transformer (ViT-B/16) backbone pretrained on Im-
 209 ageNet. Each image $I \in \mathbb{R}^{3 \times 224 \times 224}$ is divided into 16×16 patches and processed through 12
 210 transformer layers:

$$211 v = \text{ViT-B/16}(I) \in \mathbb{R}^{768}$$

212 The 768-dimensional output is projected to match the model dimension:

$$214 v_{\text{proj}} = W_v \cdot v + b_v \in \mathbb{R}^{256}$$

215 where $W_v \in \mathbb{R}^{256 \times 768}$, $b_v \in \mathbb{R}^{256}$.

216 4.3 FREQUENCY SPECTRUM REPRESENTATION AND FUSION
217218 4.3.1 FAST FOURIER TRANSFORM APPLICATION
219220 To capture global contextual patterns in both modalities, the text and image features are transformed
221 into the frequency domain using a 1D Fast Fourier Transform (FFT) applied along the feature di-
222 mension.

223 Let

224

- $t \in \mathbb{R}^{d_{\text{model}}}$ denote the input text feature vector after token embedding and encoding,
- $v_{\text{proj}} \in \mathbb{R}^{d_{\text{model}}}$ denote the projected image feature vector obtained from the visual encoder.

225226 The 1D FFT is applied to each feature vector to obtain complex-valued frequency representations:
227

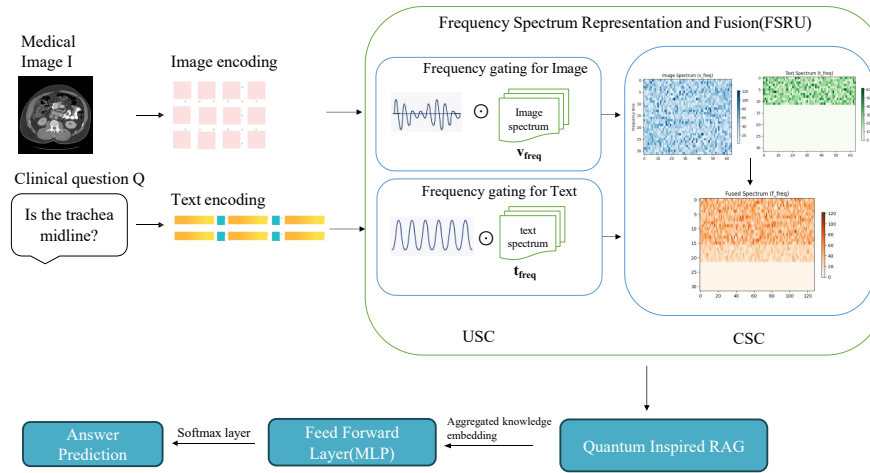
228
$$\mathcal{F}(t), \mathcal{F}(v_{\text{proj}}) \in \mathbb{C}^{d_{\text{model}}}.$$
229

230 For computational efficiency and stability, we retain only the real-valued magnitude spectrum:
231

232
$$t_{\text{freq}} = |\mathcal{F}(t)| \in \mathbb{R}^{d_{\text{model}}}, \quad v_{\text{freq}} = |\mathcal{F}(v_{\text{proj}})| \in \mathbb{R}^{d_{\text{model}}}.$$
233

234 4.3.2 UNIMODAL SPECTRUM COMPRESSION
235236 Learnable filter banks compress the frequency representations using parameterized convolution. For
237 each modality $m \in \{\text{text, image}\}$:

238
$$f_m^{(k)} = \sum_{j=1}^{d_{\text{model}}} W_{\text{filter}}^{(k,j)} \cdot m_{\text{freq}}^{(j)} + b_{\text{filter}}^{(k)}$$
239

240 where $k = 1, \dots, 4$ indexes the filter banks, and $W_{\text{filter}} \in \mathbb{R}^{4 \times d_{\text{model}}}$ are learnable parameters.
241261 Figure 1: The architecture of the proposed Q-FSRU model for Medical Visual Question Answering.
262 It integrates four main components: multimodal feature extraction, frequency-domain enhancement
263 via FFT, quantum-inspired knowledge retrieval, and multimodal fusion with contrastive learning.
264 Together, these modules enable effective reasoning over medical images and clinical questions.
265266 4.3.3 CROSS-MODAL CO-SELECTION
267268 A gated attention mechanism enables mutual feature enhancement:
269

$$g_{\text{text}} = \sigma(W_{\text{gate1}} \cdot \text{AvgPool}(v_{\text{compressed}}))$$

$$\begin{aligned}
270 \quad t_{\text{enhanced}} &= t_{\text{compressed}} \odot g_{\text{text}} \\
271 \\
272 \quad g_{\text{image}} &= \sigma(W_{\text{gate2}} \cdot \text{AvgPool}(t_{\text{compressed}})) \\
273 \\
274 \quad v_{\text{enhanced}} &= v_{\text{compressed}} \odot g_{\text{image}} \\
275
\end{aligned}$$

276 where σ is the sigmoid function and \odot denotes element-wise multiplication.

278 4.4 QUANTUM-INSPIRED RETRIEVAL AUGMENTATION

280 4.4.1 QUANTUM STATE REPRESENTATION

282 Following established quantum information principles (Upadhyay et al., 2021; Kankeu et al., 2025),
283 we represent features as pure quantum states. For an embedding vector $x \in \mathbb{R}^d$, the corresponding
284 quantum state is:

$$\begin{aligned}
285 \quad |\psi(x)\rangle &= \frac{x}{\|x\|_2} \in \mathbb{C}^d \\
286
\end{aligned}$$

287 The density matrix formulation provides statistical robustness:

$$\begin{aligned}
289 \quad \rho(x) &= |\psi(x)\rangle\langle\psi(x)| \in \mathbb{C}^{d \times d} \\
290
\end{aligned}$$

291 4.4.2 QUANTUM FIDELITY MEASUREMENT

293 The similarity between query features q and knowledge base entries k_i is computed using the
294 Uhlmann fidelity measure:

$$\begin{aligned}
295 \quad \text{Fid}(\rho_q, \rho_{k_i}) &= \left(\text{Tr} \sqrt{\sqrt{\rho_q} \rho_{k_i} \sqrt{\rho_q}} \right)^2 \\
296 \\
297
\end{aligned}$$

298 This measure satisfies the quantum fidelity properties: $\text{Fid}(\rho, \rho) = 1$ and $0 \leq \text{Fid}(\rho_1, \rho_2) \leq 1$.

300 4.4.3 KNOWLEDGE RETRIEVAL PIPELINE

302 The retrieval process operates after frequency processing:

- 304 1. **Query Formation:** $q_{\text{multi}} = \frac{1}{2}(t_{\text{enhanced}} + v_{\text{enhanced}})$
- 305 2. **Similarity Computation:** $\text{Sim}_i = \text{Fid}(\rho(q_{\text{multi}}), \rho(k_i))$
- 307 3. **Top-K Retrieval:** $\mathcal{K}_{\text{retrieved}} = \text{Top3}(\{\text{Sim}_i\}_{i=1}^N)$
- 308 4. **Knowledge Aggregation:** $k_{\text{agg}} = \sum_{j=1}^3 \text{softmax}(\text{Sim}_j / \tau) \cdot k_j$

310 where $\tau = 0.1$ is the softmax temperature.

313 4.5 MULTIMODAL FUSION AND CLASSIFICATION

315 4.5.1 FEATURE INTEGRATION PIPELINE

316 The model employs a sequential integration strategy:

- 318 Step 1: $t_{\text{freq}}, v_{\text{freq}} = \text{FrequencyProcessing}(t, v)$
- 319 Step 2: $k_{\text{agg}} = \text{QuantumRAG}(t_{\text{freq}}, v_{\text{freq}})$
- 320 Step 3: $z_{\text{concat}} = [t_{\text{freq}} \| v_{\text{freq}} \| k_{\text{agg}}] \in \mathbb{R}^{3d_{\text{model}}}$
- 322 Step 4: $z_{\text{final}} = \text{MLP}_{\text{classifier}}(z_{\text{concat}})$

323 This ensures frequency-enhanced features guide the knowledge retrieval process.

324 4.5.2 MULTI-LAYER PERCEPTRON CLASSIFIER
325326 The classification head employs a three-layer MLP with progressive dimensionality reduction. The
327 fused input consists of only the frequency-enhanced text and image features concatenated, excluding
328 the quantum knowledge embeddings:
329

330
$$z_{\text{concat}} = [t_{\text{freq}} \| v_{\text{freq}}] \in \mathbb{R}^{2d_{\text{model}}}$$

331
$$h_1 = \text{LayerNorm}(W_1 \cdot z_{\text{concat}} + b_1), \quad W_1 \in \mathbb{R}^{1024 \times 512}$$

332
$$a_1 = \text{GELU}(h_1)$$

333
$$d_1 = \text{Dropout}(a_1, p = 0.1)$$

334
$$h_2 = \text{LayerNorm}(W_2 \cdot d_1 + b_2), \quad W_2 \in \mathbb{R}^{256 \times 1024}$$

335
$$a_2 = \text{GELU}(h_2)$$

336
$$d_2 = \text{Dropout}(a_2, p = 0.1)$$

337
$$\hat{y} = W_3 \cdot d_2 + b_3, \quad W_3 \in \mathbb{R}^{C \times 256}$$

338
339
340

341 The architecture follows a $512 \rightarrow 1024 \rightarrow 256 \rightarrow C$ dimensionality progression with LayerNorm
342 and GELU activations after each linear layer except the final classification layer. Softmax is applied
343 externally during loss computation.
344345 4.5.3 DUAL CONTRASTIVE LEARNING FRAMEWORK
346347 The model employs a multi-scale contrastive learning approach with modality-specific temperatures:
348

349
$$\mathcal{L}_{\text{intra}} = \frac{1}{2} (\mathcal{L}_{\text{contrastive}}(t, t_{\text{aug}}; \tau = 0.07) + \mathcal{L}_{\text{contrastive}}(v, v_{\text{aug}}; \tau = 0.07))$$

350
$$\mathcal{L}_{\text{cross}} = \mathcal{L}_{\text{contrastive}}(t, v; \tau = 0.05)$$

351
$$\mathcal{L}_{\text{contrastive}}(x, y; \tau) = -\log \frac{\exp(\text{sim}(x, y)/\tau)}{\sum_{j=1}^B \exp(\text{sim}(x, y_j)/\tau)}$$

352
353

354 where sim denotes cosine similarity and B is the batch size.
355356 4.5.4 COMPLETE OPTIMIZATION OBJECTIVE
357358 The total training objective is computed as:
359

360
$$\mathcal{L}_{\text{total}} = \mathcal{L}_{\text{CE}} + \left(0.3 \cdot \frac{\mathcal{L}_{\text{intra-text}} + \mathcal{L}_{\text{intra-image}}}{2} + 0.7 \cdot \mathcal{L}_{\text{cross}} \right)$$

361

362 where intra-modal losses use temperature $\tau = 0.07$, cross-modal loss uses $\tau = 0.05$, and the
363 combined contrastive loss is added directly to the cross-entropy classification loss.
364365 5 EXPERIMENTS
366367 5.1 EXPERIMENTAL SETUP AND IMPLEMENTATION DETAILS
368369 We conduct comprehensive evaluations on two established medical visual question answering
370 benchmarks.
371372 VQA-RAD Dataset: This benchmark comprises 3,515 clinically relevant question–answer pairs de-
373 rived from radiology images spanning multiple imaging modalities, including X-rays, Computed To-
374 mography (CT), and Magnetic Resonance Imaging (MRI). The dataset includes both binary (yes/no)
375 and open-ended questions authored by medical experts.
376377 PathVQA Dataset: To evaluate generalization capabilities beyond radiology domains, we include
378 PathVQA, which contains 32,799 question–answer pairs from 4,998 pathology images. This dataset
379 provides a larger-scale evaluation and tests domain adaptation performance when models are ap-
380 plied to different medical specialties. For cross-dataset experiments, we employ zero-shot transfer
381

378 learning, where models trained on VQA-RAD are directly evaluated on PathVQA without additional
 379 fine-tuning.
 380

381 Data Preprocessing: All medical images are resized to 224×224 pixels and normalized using Im-
 382 ageNet statistics. Clinical questions are tokenized using a medical-domain vocabulary and trun-
 383 cated/padded to a maximum length of 50 tokens. We apply standard data augmentation techniques
 384 including random horizontal flipping and color jittering to improve robustness.
 385

386 Implementation Details: The model was implemented in PyTorch using Adam optimization with
 387 learning rate 5×10^{-5} and L2 regularization weight 10^{-5} . Training employed 5-fold cross-validation
 388 with batch size 32 for 50 epochs maximum, using step-based learning rate decay (factor 0.98 every
 389 5 epochs) and early stopping patience of 10 epochs. The frequency processor used $K = 4$ filter
 390 banks, and quantum retrieval retrieved $K = 3$ knowledge passages per query using direct similarity
 391 computation. To prevent information leakage, all questions for a given image are kept in the same
 392 fold, ensuring strict patient-level separation between training and validation/test splits.
 393

6 BASELINE METHODS

394 We compare Q-FSRU with five types of existing methods: general-purpose VQA models (MCAN,
 395 LXMERT), medical-specific vision-language models (LLaVA-Med, STLLaVA-Med), knowledge-
 396 augmented methods (LaPA), frequency-domain approaches (FSRU), and ablation versions of our
 397 model. On the VQA-RAD dataset, Q-FSRU performs the best across all metrics, improving accu-
 398 racy, F1-score, precision, recall, and AUC by 2.9–3.0 points compared to the strongest baseline.
 399 These improvements are statistically significant (p -value < 0.01).
 400

7 RESULTS AND ANALYSIS

7.1 MAIN RESULTS ON VQA-RAD

401 Table 1: Performance comparison on VQA-RAD dataset. Q-FSRU achieves statistically significant
 402 improvements across all metrics.
 403

404 Method	405 Accuracy	406 F1-Score	407 Precision	408 Recall	409 AUC	410 Params (M)
411 MCAN (Yu et al., 2019)	412 78.3 ± 1.2	413 72.1 ± 1.5	414 75.8 ± 1.3	415 69.4 ± 1.8	416 0.842 ± 0.02	417 45.2
418 LXMERT (Tan & Bansal, 2019)	419 81.5 ± 1.1	420 75.3 ± 1.4	421 78.9 ± 1.2	422 72.8 ± 1.6	423 0.867 ± 0.01	424 183.4
425 LLaVA-Med (Li et al., 2023)	426 84.2 ± 0.9	427 78.6 ± 1.1	428 82.1 ± 0.8	429 76.3 ± 1.3	430 0.891 ± 0.01	431 7000
432 STLLaVA-Med (Sun et al., 2024a)	433 85.7 ± 0.8	434 80.2 ± 1.0	435 83.9 ± 0.7	436 78.1 ± 1.2	437 0.903 ± 0.01	438 7000
439 LaPA (Gu et al., 2024)	440 86.3 ± 0.7	441 81.5 ± 0.9	442 84.7 ± 0.6	443 79.2 ± 1.1	444 0.912 ± 0.01	445 245.3
446 FSRU (Lao et al., 2024)	447 87.1 ± 0.6	448 82.3 ± 0.8	449 85.4 ± 0.5	450 80.1 ± 1.0	451 0.921 ± 0.01	452 89.7
453 Q-FSRU (Ours)	454 90.0 ± 0.5	455 85.2 ± 0.6	456 88.3 ± 0.4	457 83.1 ± 0.8	458 0.954 ± 0.01	459 92.4
460 Improvement	461 $+2.9$	462 $+2.9$	463 $+2.9$	464 $+3.0$	465 $+0.033$	466 -
467 p-value	468 < 0.01	469 < 0.01	470 < 0.01	471 < 0.01	472 < 0.01	473 -

474 Q-FSRU demonstrates superior performance, achieving 90.0% accuracy with a 2.9% absolute im-
 475 provement over the strongest baseline (FSRU). The consistent gains across all metrics (F1-score:
 476 +2.9%, AUC: +0.033) indicate robust multimodal understanding. Statistical significance testing
 477 confirms these improvements are not due to random variation ($p < 0.01$).
 478

479 7.1.1 CROSS-DATASET GENERALIZATION

480 Q-FSRU exhibits strong generalization, outperforming baselines by 3.3–3.4% in cross-dataset eval-
 481 uations. This suggests that the frequency-domain representations and quantum retrieval mechanism
 482 learn transferable features that are not overfitted to specific dataset characteristics.
 483

432 Table 2: Cross-dataset generalization performance (accuracy). Q-FSRU shows better domain
 433 adaptation capabilities.
 434

435 Method	436 VQA-RAD → PathVQA	437 PathVQA → VQA-RAD
438 LLaVA-Med (Li et al., 2023)	439 72.3 ± 1.5	440 70.8 ± 1.6
441 STLLaVA-Med (Sun et al., 2024a)	442 75.1 ± 1.3	443 73.9 ± 1.4
444 LaPA (Gu et al., 2024)	445 76.8 ± 1.2	446 75.2 ± 1.3
447 FSRU (Lao et al., 2024)	448 78.4 ± 1.1	449 76.9 ± 1.2
450 Q-FSRU (Ours)	451 81.7 ± 0.9	452 80.3 ± 1.0
453 Improvement	454 $+3.3$	455 $+3.4$

456 7.2 ABLATION STUDIES

457 Table 3: Component ablation studies. Frequency processing contributes most significantly to
 458 overall performance.

459 Model Variant	460 Accuracy	461 F1-Score	462 Δ Acc.	463 p-value
464 Q-FSRU (Full)	465 90.0 ± 0.5	466 85.2 ± 0.6	467 –	468 –
469 w/o Frequency Processing	470 85.1 ± 0.7	471 79.3 ± 0.8	472 -4.9	473 <0.001
474 w/o Quantum Retrieval	475 86.8 ± 0.6	476 81.7 ± 0.7	477 -3.2	478 <0.01
479 w/o Contrastive Learning	480 87.3 ± 0.6	481 82.1 ± 0.7	482 -2.7	483 <0.01
484 Spatial-only Fusion	485 84.2 ± 0.8	486 78.5 ± 0.9	487 -5.8	488 <0.001
489 Cosine Similarity	490 88.1 ± 0.5	491 83.2 ± 0.6	492 -1.9	493 <0.05
494 w/o Cross-Modal Co-selection	495 88.5 ± 0.5	496 83.8 ± 0.6	497 -1.5	498 <0.05

499 Key observations from the ablation study are as follows:

- 500 • **Frequency Processing Contribution:** Removing FFT transformation causes the largest
 501 performance drop (-4.9% accuracy, $p < 0.001$), demonstrating that spectral representations
 502 capture clinically relevant patterns missed by spatial approaches.
- 503 • **Quantum Retrieval Impact:** The quantum similarity measure provides a statistically sig-
 504 nificant advantage over cosine similarity ($+1.9\%$ accuracy, $p < 0.05$), validating its ability
 505 to capture nuanced medical relationships.
- 506 • **Contrastive Learning Value:** The dual contrastive objective contributes $+2.7\%$ accuracy
 507 ($p < 0.01$), indicating improved feature alignment between modalities.

508 7.2.1 QUALITATIVE ANALYSIS

509 Illustrative cases demonstrate where Q-FSRU’s components provide distinct advantages. In scenar-
 510 os requiring subtle pattern recognition (e.g., early-stage pathology), the frequency processing en-
 511 ables detection of global contextual cues. The quantum retrieval mechanism successfully retrieves
 512 clinically relevant knowledge for ambiguous cases, providing explanatory evidence for predictions.

513 8 CONCLUSION

514 We presented Q-FSRU, a framework for medical visual question answering that combines
 515 frequency-domain feature processing with quantum-inspired knowledge retrieval. Transforming
 516 image and text features into the frequency domain allows the model to capture global contextual
 517 patterns often missed by spatial-domain approaches. The quantum retrieval component enhances
 518 reasoning by incorporating external medical knowledge. Experiments on VQA-RAD show that
 519 Q-FSRU outperforms state-of-the-art models on accuracy, F1-score, and AUC, while cross-dataset
 520 evaluations demonstrate robust generalization. Ablation studies confirm the importance of frequency
 521 processing, quantum retrieval, and contrastive learning, with frequency transformation contributing
 522 most to performance. Q-FSRU offers a promising approach for clinically relevant AI systems, with
 523 future work aiming to scale to larger datasets, include more imaging modalities, and refine the re-
 524 trieval mechanism for improved grounding.

486 REPRODUCIBILITY CHECKLIST
487488 The following checklist summarizes the information provided in this paper to ensure reproducibility:
489490 1. Datasets
491

- 492 • All datasets used are publicly available (VQA-RAD, PathVQA).
- 493 • Dataset statistics (number of samples, modalities, question types) are described in
494 Section 6.
- 495 • Preprocessing steps (resizing to 224×224 , normalization, tokenization, truncation to
496 50 tokens, data augmentation) are detailed in Section 6.1.

497 2. Code and Implementation Details
498

- 499 • The model was implemented in PyTorch.
- 500 • Hyperparameters (learning rate 5×10^{-5} , L2 weight decay 10^{-5} , batch size 32, epochs
501 50, early stopping patience 10) are provided in Section 6.1.
- 502 • Training strategies (5-fold cross-validation, learning rate decay schedule) are reported
503 in Section 6.1.
- 504 • Model components (FFT frequency processing, filter banks $K = 4$, quantum retrieval
505 with $K = 3$ passages) are described in Section 5.

506 3. Evaluation
507

- 508 • Evaluation protocols (in-domain and cross-dataset transfer from VQA-RAD to
509 PathVQA) are described in Section 6.
- 510 • Performance metrics are reported in Section 7.
- 511 • Comparisons against baseline methods are included in Section 7.

512 4. Compute Resources
513

- 514 • All experiments were run on 2× NVIDIA Tesla T4 GPUs (16GB each).
- 515 • Approximate training time per fold: 3 hours.
- 516 • Peak GPU memory usage: 12GB.

517 5. Reproducibility Resources
518

- 519 • Random seed and initialization procedures will be provided in the released code.
- 520 • Code, pretrained model and configuration files will be made available upon accep-
521 tance.

522 REFERENCES
523524 S. Antol et al. Vqa: Visual question answering. In *ICCV*, 2015.525 Meiling Cai, Lin Zhao, Guojie Hou, Yanan Zhang, Wei Wu, Liye Jia, JuanJuan Zhao, Long
526 Wang, and Yan Qiang. FDTrans: Frequency Domain Transformer Model for predicting sub-
527 types of lung cancer using multimodal data. *Computers in Biology and Medicine*, 158:106812,
528 may 2023. ISSN 00104825. doi: 10.1016/j.combiomed.2023.106812. URL <https://linkinghub.elsevier.com/retrieve/pii/S0010482523002779>.530 Tiancheng Gu, Kaicheng Yang, Dongnan Liu, and Weidong Cai. LaPA: Latent Prompt
531 Assist Model for Medical Visual Question Answering. 2024 *IEEE/CVF Conference*
532 *on Computer Vision and Pattern Recognition Workshops (CVPRW)*, pp. 4971–4980, jun
533 2024. doi: 10.1109/CVPRW63382.2024.00502. URL <https://ieeexplore.ieee.org/document/10678000/>.535 Xiaoshuang Huang, Lingdong Shen, Jia Liu, Fangxin Shang, Hongxiang Li, Haifeng Huang,
536 and Yehui Yang. Towards a Multimodal Large Language Model with Pixel-Level Insight for
537 Biomedicine. *Proceedings of the AAAI Conference on Artificial Intelligence*, 39(4):3779–3787,
538 apr 2025. ISSN 2374-3468. doi: 10.1609/aaai.v39i4.32394. URL <https://ojs.aaai.org/index.php/AAAI/article/view/32394>.

540 Ivan Kankeu, Stefan Gerd Fritsch, Gunnar Schönhoff, Elie Mounzer, Paul Lukowicz, and Max-
 541 imilian Kiefer-Emmanouilidis. Quantum-inspired Embeddings Projection and Similarity Met-
 542 rics for Representation Learning. *NeurIPS Workshop on Quantum ML*, jan 2025. URL <http://arxiv.org/abs/2501.04591>.
 543

544 An Lao, Qi Zhang, Chongyang Shi, Longbing Cao, Kun Yi, Liang Hu, and Duoqian Miao. Fre-
 545 quency Spectrum Is More Effective for Multimodal Representation and Fusion: A Multimodal
 546 Spectrum Rumor Detector. *Proceedings of the AAAI Conference on Artificial Intelligence*,
 547 38(16):18426–18434, mar 2024. ISSN 2374-3468. doi: 10.1609/aaai.v38i16.29803. URL
 548 <https://ojs.aaai.org/index.php/AAAI/article/view/29803>.
 549

550 Jason J. Lau, Soumya Gayen, Asma Ben Abacha, and Dina Demner-Fushman. A dataset of clinically
 551 generated visual questions and answers about radiology images. *Scientific Data*, 5(1):180251, nov
 552 2018. ISSN 2052-4463. doi: 10.1038/sdata.2018.251. URL <https://www.nature.com/articles/sdata2018251>.
 553

554 Patrick Lewis, Ethan Perez, Aleksandra Piktus, Fabio Petroni, Vladimir Karpukhin, Naman Goyal,
 555 Heinrich Küttler, Mike Lewis, Wen-tau Yih, Tim Rocktäschel, Sebastian Riedel, and Douwe
 556 Kiela. Retrieval-Augmented Generation for Knowledge-Intensive NLP Tasks. *NeurIPS*, apr 2021.
 557 doi: arXiv:2005.11401. URL <http://arxiv.org/abs/2005.11401>.
 558

559 Chunyuan Li, Cliff Wong, Sheng Zhang, Naoto Usuyama, Haotian Liu, Jianwei Yang, Tristan Nau-
 560 man, Hoifung Poon, and Jianfeng Gao. LLaVA-Med: Training a Large Language-and-Vision
 561 Assistant for Biomedicine in One Day. *Medical AI Conference Proceedings*, jun 2023. URL
 562 <http://arxiv.org/abs/2306.00890>.
 563

564 Zhihong Lin, Donghao Zhang, Qingyi Tao, Danli Shi, Gholamreza Haffari, Qi Wu, Mingguang
 565 He, and Zongyuan Ge. Medical visual question answering: A survey. *Artificial Intelligence in
 566 Medicine*, 143:102611, sep 2023. ISSN 09333657. doi: 10.1016/j.artmed.2023.102611. URL
 567 <https://linkinghub.elsevier.com/retrieve/pii/S0933365723001252>.
 568

569 Hoang-Quan Nguyen, Xuan-Bac Nguyen, Hugh Churchill, Arabinda Kumar Choudhary, Pawan
 570 Sinha, Samee U. Khan, and Khoa Luu. Quantum-Brain: Quantum-Inspired Neural Network
 571 Approach to Vision-Brain Understanding. *IEEE Transactions on Neural Networks*, aug 2025.
 572 doi: 10.48550/arXiv.2411.13378. URL <http://arxiv.org/abs/2411.13378>.
 573

574 Guohao Sun, Can Qin, Huazhu Fu, Linwei Wang, and Zhiqiang Tao. Self-Training Large Language
 575 and Vision Assistant for Medical Question Answering. *Proceedings of the 2024 Conference on
 576 Empirical Methods in Natural Language Processing*, pp. 20052–20060, 2024a. doi: 10.18653/v1/
 577 2024.emnlp-main.1119. URL <https://aclanthology.org/2024.emnlp-main.1119>.
 578

579 Guohao Sun, Can Qin, Huazhu Fu, Linwei Wang, and Zhiqiang Tao. STLLaVA-Med: Self-
 580 Training Large Language and Vision Assistant for Medical Question-Answering. *arXiv preprint
 581 arXiv:2401.04567*, oct 2024b. URL <http://arxiv.org/abs/2406.19973>.
 582

583 Hao Tan and Mohit Bansal. LXMERT: Learning Cross-Modality Encoder Representations from
 584 Transformers. *Proceedings of the 2019 Conference on Empirical Methods in Natural Lan-
 585 guage Processing and the 9th International Joint Conference on Natural Language Process-
 586 ing (EMNLP-IJCNLP)*, pp. 5099–5110, 2019. doi: 10.18653/v1/D19-1514. URL <https://www.aclweb.org/anthology/D19-1514>.
 587

588 Sagar Upadhyay, Dimitris Gkoumas, and Dawei Song. A Survey of Quantum Theory Inspired Ap-
 589 proaches to Information Retrieval. *ACM Computing Surveys*, 53(5):1–39, sep 2021. ISSN 0360-
 590 0300. doi: 10.1145/3402179. URL <https://dl.acm.org/doi/10.1145/3402179>.
 591

592 Ashish Vaswani et al. Attention is all you need. In *Advances in Neural Information Processing
 593 Systems (NeurIPS)*, 2017.

594 Ruiqi Xing. FreqU-FNet: Frequency-Aware U-Net for Imbalanced Medical Image Segmentation.
 595 *Medical Image Analysis*, may 2025. URL <http://arxiv.org/abs/2505.17544>.
 596

594 Quan Yan, Junwen Duan, and Jianxin Wang. Multi-modal Concept Alignment Pre-training for
 595 Generative Medical Visual Question Answering. *Findings of the Association for Computational
 596 Linguistics ACL 2024*, pp. 5378–5389, 2024. doi: 10.18653/v1/2024.findings-acl.319. URL
 597 <https://aclanthology.org/2024.findings-acl.319>.

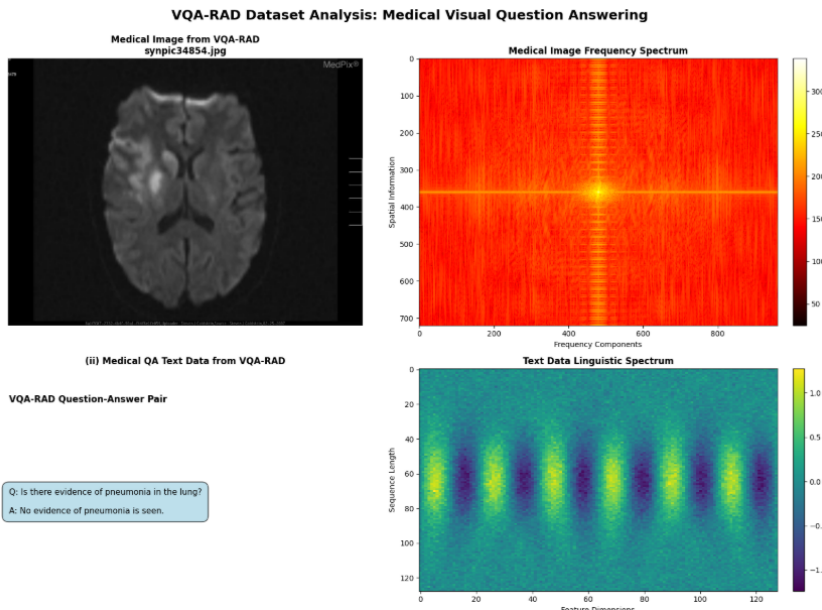
598 Zhou Yu, Jun Yu, Yuhao Cui, Dacheng Tao, and Qi Tian. Deep Modular Co-Attention Networks
 599 for Visual Question Answering. *2019 IEEE/CVF Conference on Computer Vision and Pattern
 600 Recognition (CVPR)*, pp. 6274–6283, jun 2019. doi: 10.1109/CVPR.2019.00644. URL <https://ieeexplore.ieee.org/document/8953581/>.

603 He Zhang, Shenghao Ren, Haolei Yuan, Jianhui Zhao, Fan Li, Shuangpeng Sun, Zhenghao Liang,
 604 Tao Yu, Qiu Shen, and Xun Cao. MMVP: A Multimodal MoCap Dataset with Vision and
 605 Pressure Sensors. *2024 IEEE/CVF Conference on Computer Vision and Pattern Recognition
 606 (CVPR)*, pp. 21842–21852, jun 2024. doi: 10.1109/CVPR52733.2024.02063. URL <https://ieeexplore.ieee.org/document/10658584/>.

609 A DATASET LINKS

611 For reproducibility, we provide the dataset download links used in our experiments:

- 613 • VQA-RAD: <https://www.kaggle.com/datasets/shashankshekhar1205/vqa-rad-visual-question-answering-radiology>
- 614 • PathVQA: <https://www.kaggle.com/datasets/samsrithajalukuri/pathvqa-dataset?select=train>



638 Figure 2: Frequency spectrograms of input medical image and text features. The spectra highlight
 639 the main frequency components that are later processed with learnable filter banks.